

Research Paper

Targeted Radionuclide Therapy with A ^{177}Lu -labeled Anti-HER2 Nanobody

Matthias D'Huyvetter^{1,2}, Cécile Vincke^{3,4}, Catarina Xavier², An Aerts¹, Nathalie Impens¹, Sarah Baatout¹, Hendrik De Raeve^{5,6}, Serge Muyltermans^{3,4}, Vicky Caveliers^{2,7}, Nick Devoogdt^{2,4}, Tony Lahoutte^{2,7}

1. Radiobiology Unit, Molecular and Cellular Biology Expert Group, Belgian Nuclear Research Center (SCK•CEN), Mol, Belgium.
2. In vivo Cellular and Molecular Imaging Laboratory (ICMI), Vrije Universiteit Brussel (VUB), Brussels, Belgium.
3. Structural Biology Research Center, Vlaams Instituut voor Biotechnologie (VIB), Brussels, Belgium.
4. Laboratory of Cellular and Molecular Immunology, Vrije Universiteit Brussel (VUB), Brussels, Belgium.
5. Department of Pathology, OLV Hospital Aalst, Aalst, Belgium.
6. Department of Pathology, UZ Brussel, Brussels, Belgium.
7. Department of Nuclear Medicine, UZ Brussel, Brussels, Belgium.

#Share senior authorship.

 Corresponding author: Matthias D'Huyvetter, MSc, In vivo Cellular and Molecular Imaging Laboratory, Vrije Universiteit Brussel, Laarbeeklaan 103, 1090 Brussels, Belgium; Tel (+32) 2 477 4991; E-mail: mdhuyvet@vub.ac.be.

© Ivyspring International Publisher. This is an open-access article distributed under the terms of the Creative Commons License (<http://creativecommons.org/licenses/by-nc-nd/3.0/>). Reproduction is permitted for personal, noncommercial use, provided that the article is in whole, unmodified, and properly cited.

Received: 2013.11.18; Accepted: 2014.03.24; Published: 2014.04.25

Abstract

RIT has become an attractive strategy in cancer treatment, but still faces important drawbacks due to poor tumor penetration and undesirable pharmacokinetics of the targeting vehicles. Smaller radiolabeled antibody fragments and peptides feature highly specific target accumulation, resulting in low accumulation in healthy tissue, except for the kidneys. Nanobodies are the smallest (MW < 15 kDa) functional antigen-binding fragments that are derived from heavy chain-only camelid antibodies.

Here, we show that the extend of kidney retention of nanobodies is predominantly dictated by the number of polar residues in the C-terminal amino acid tag. Three nanobodies were produced with different C-terminal amino-acid tag sequences (Myc-His-tagged, His-tagged, and untagged). Dynamic planar imaging of Wistar rats with ^{111}In -DTPA-nanobodies revealed that untagged nanobodies showed a 70 % drop in kidney accumulation compared to Myc-His-tagged nanobodies at 50 min p.i.. In addition, coinfusion of untagged nanobodies with the plasma expander Gelofusin led to a final reduction of 90 %. Similar findings were obtained with different ^{177}Lu -DTPA-2Rs15d nanobody constructs in HER2^{pos} tumor xenografted mice at 1 h p.i.. Kidney accumulation decreased 88 % when comparing Myc-His-tagged to untagged 2Rs15d nanobody, and 95 % with a coinfusion of Gelofusin, without affecting the tumor targeting capacity. Consequently, we identified a generic method to reduce kidney retention of radiolabeled nanobodies. Dosimetry calculations of Gelofusin-coinfused, untagged ^{177}Lu -DTPA-2Rs15d revealed a dose of 0.90 Gy/MBq that was delivered to both tumor and kidneys and extremely low doses to healthy tissues. In a comparative study, ^{177}Lu -DTPA-Trastuzumab supplied 6 times more radiation to the tumor than untagged ^{177}Lu -DTPA-2Rs15d, but concomitantly also a 155, 34, 80, 26 and 4180 fold higher radioactivity burden to lung, liver, spleen, bone and blood.

Most importantly, nanobody-based targeted radionuclide therapy in mice bearing small established HER2^{pos} tumors led to an almost complete blockade of tumor growth and a significant difference in event-free survival between the treated and the control groups ($P < 0.0001$). Based on histology analyses, no evidence of renal inflammation, apoptosis or necrosis was obtained.

In conclusion, these data highlight the importance of the amino acid composition of the nanobody's C-terminus, as it has a predominant effect on kidney retention. Moreover, we show successful nanobody-based targeted radionuclide therapy in a xenograft model and highlight the potential of radiolabeled nanobodies as a valuable adjuvant therapy candidate for treatment of minimal residual and metastatic disease.

Key words: HER2, nanobody, targeted radionuclide therapy, ^{177}Lu -Lutetium.

Introduction

RIT has become an attractive therapeutic application, as it has the ability to target both the primary tumor site as well as disseminated diseased tissue. However, poor tumor penetration and undesirable pharmacokinetics limit the efficacy of RIT with radiolabeled mAbs. Nowadays, only two agents are approved for commercial use, Yttrium-90 ibritumomab (Zevalin, Biogen-Idec Pharmaceuticals) and Iodine-131 tositumomab (BEXXAR, GlaxoSmithKline), both used to treat indolent B-cell lymphoma.

The treatment of epithelial-based tumors is more difficult, as the actual dose delivered to tumors remains often inadequate, due to the dose-limiting toxicity to healthy tissues (1, 2). However, recent advances in the development of recombinant protein or peptide-derived targeting probes highlight the potential of overcoming these limitations. Indeed, many small radiolabeled antibody fragments and peptides feature highly specific but moderate target accumulation and are rapidly cleared from the blood, resulting in low accumulation in healthy tissue. However, since kidneys are the major excretion routes, intense accumulation of radioactivity in the renal cortical region is observed. High kidney retention is a well-described phenomenon (3,4). Although small size facilitates rapid clearance through the glomeruli in the kidneys, it is followed by a firm interaction with the negatively-charged lumen of the tubular system. This is attributed to the endocytic receptors megalin and cubulin, which are highly present in the renal proximal tubuli and are involved in the process of protein reabsorption. For targeted radiotherapy using long-lived radioisotopes, the intense kidney retention becomes a major dosimetric concern in terms of renal tissue toxicity and often limits its applicability. Radiation nephropathy has indeed been observed in several patients after PRRT using radiolabeled somatostatin analogues (5-7). Recently, several countermeasures were described to reduce kidney retention of radiolabeled targeting probes (8-10), of which positively charged amino acid and/or Gelofusin coinjections became standard practice in PRRT. Gelofusin consists of succinylated bovine gelatin molecules and is clinically used as a plasma expander. In the past, it

has been shown to enhance excretion of megalin ligands. Moreover, kidney retention of radiolabeled octreotide analogs is reduced with about 45 % upon infusion of Gelofusin. A combination of Gelofusin and L-lysine could reduce kidney uptake even further (9).

Nanobodies are the smallest antigen-binding fragments (MW around 14 kDa) derived from heavy chain-only antibodies naturally occurring in camelids (11). These minimal-sized recombinant antigen-binding fragments are rapidly cleared from blood, highly soluble in aqueous solution and highly robust. They associate specifically and efficiently with their cognate target (12). Their potential as *in vivo* diagnostic tracers is well documented, targeting a variety of extracellular tumor cell biomarkers such as CEA (13), EGFR (14), HER2 (15,16) and PSMA (17).

In this study, we focus on nanobody-based targeted radionuclide therapy of HER2^{pos} xenografted tumors, using the therapeutic radionuclide ^{177}Lu ($T_{1/2} = 6.72$ days, $\langle E_{\beta} \rangle = 133$ keV). HER2 is overexpressed in a series of human cancer types such as breast, ovarian, colorectal and urothelial carcinomas (18). Its incidence for breast cancer ranges around 20-30 % and is often associated with a higher recurrence rate and a shorter time to relapse (19). Recently we reported the identification and characterization of an anti-HER2 nanobody, referred to as 2Rs15d, for clinical translation. Its selection was based on a complete screening of 38 anti-HER2 nanobodies that were derived from heavy chain-only antibodies and raised by immunizing a dromedary (15). To this end, nanobodies were ^{99m}Tc -labeled by means of site-specific conjugation of a ^{99m}Tc -tricarbonyl core at the imidazole residues of the C-terminal His-tag of the protein. Subsequently, the characterisation of ^{68}Ga -labeled 2Rs15d was also described in terms of clinical immuno-PET imaging (16). Finally, the His-tagged anti-HER2 2Rs15d was also radiolabeled with ^{177}Lu and biodistribution was assessed in xenografted mice (20). In the latter study we demonstrated that the bifunctional chelator 1B4M-DTPA was the preferred chelator for ^{177}Lu -labeling as it exhibited the most favorable biodistribution. Overall, specific tumor targeting and low background tissue uptake was observed but, as expected, kidney accumulation was predominant and

persistent. In the current study we therefore aim to optimize the nanobody format for reduced kidney retention. Next, its biodistribution in healthy wistar rats and a xenografted mouse model were assessed, followed by a dosimetric analysis. Finally, nanobody-based targeted radionuclide therapy was performed in mice bearing HER2^{pos} tumors.

Materials and Methods

Cell line and culture conditions

The human ovarian cancer cell line SKOV3 (HER2^{pos}) was obtained from American Type Culture Collection (ATCC, Manassas, VA, USA). SKOV3-LUC (HER2^{pos}/Luciferase^{pos}) was made in-house by transfecting the SKOV3 cells with luciferase-encoding lentiviral particles, as described previously (21). SKOV3 cells were cultured using McCoy's 5A medium, SKOV3-LUC in DMEM medium. Both media were enriched with 10 % fetal bovine serum, L-Glutamine (2 mM), 100 U/mL of penicillin and 0.1 mg/mL streptomycin. Cells were grown in a humidified atmosphere with 5 % CO₂ at 37 °C. Prior to use for *in vitro* and *in vivo* purposes, cells were detached by using trypsin-EDTA. All media and supplements were obtained from Life Technologies (Paisley, UK).

Nanobody production and purification

Anti-HER2 nanobodies 2Rs15d, 2Rb17c and 1R136b were produced with 3 types of C-terminal amino acid tags: untagged (nanobody), His-tag (nanobody-HHHHHH), and Myc-His-tag (nanobody-AAAEQKLISEEDLNGAA-HHHHHH). Nanobodies were expressed in bacteria and purified, as described previously (22). Briefly, the sequences were re-cloned into an expression vector either containing a His-tag (pHEN6), a Myc-His-tag (pHEN18), or devoid of any tag (pHEN21). The recombinant vectors were transformed into *E. coli* WK6 cells for nanobody expression and extraction of periplasmic proteins. His- and Myc-His-tagged nanobodies were further purified by affinity chromatography on His-Select Nickel Affinity Gel (GE Healthcare). Untagged control nanobody BclI10, recognizing a bacterial enzyme (23), and both untagged 2Rb17c and 1R136b were purified on protein A Sepharose beads (GE Healthcare). The production of untagged 2Rs15d was performed according to Xavier and coworkers (16). Final purification of all nanobodies was performed through size-exclusion chromatography using Superdex 75 16/60 columns (GE Healthcare) in PBS. Protein purity and integrity were evaluated using SEC on Superdex 75 10/30 (GE Healthcare) in PBS, at flow rate 0.5 mL/min. In addition, ESI-Q-ToF-MS (Waters, Micromass) was performed, in positive mode.

Nanobody sequence analysis

The impact of the C-terminal deviations on the polarity of a nanobody was estimated with the Zimmerman polarity score plot (24). In short, amino acids in the nanobody sequence were given a polarity index value based on the dipole moments of the side chains. These values were then plotted with Graphpad Prism.

Conjugation of IB4M-DTPA and CHX-A''-DTPA to nanobodies

A 10-fold molar excess of bifunctional chelator IB4M-DTPA (for ¹⁷⁷Lu) or CHX-A''-DTPA (for ¹¹¹In) was conjugated for 3 h at RT to the free ε-amino-groups of lysines in the nanobodies in 600 μL of 0.05 M sodium carbonate buffer (pH 8.5). The conjugation reaction was quenched by reducing the pH of the mixture to pH 7.0. Nanobody-chelator was purified on Superdex 75 10/30 (GE Healthcare) in 0.1 M ammonium acetate buffer pH 7.0. The mean degree of conjugation was evaluated with ESI-Q-ToF-MS (Waters, Micromass), in positive mode.

Preparation of ¹¹¹In- and ¹⁷⁷Lu-DTPA-nanobodies

Nanobodies were labeled with ¹⁷⁷Lu as previously described (20). Carrier-free ¹⁷⁷Lu was obtained from ITG (Garching, Germany) as a chloride solution, with a specific activity of 3000 GBq/mg. Radiolabeling with ¹¹¹In was performed similarly. ¹¹¹InCl₃ was purchased from Mallinckrodt (Petten, The Netherlands) with a specific activity of 1850 GBq/mg.

The necessary amount of ¹⁷⁷Lu/¹¹¹In was added to a test vial containing metal-free 0.1 M ammonium acetate buffer pH 5.0, to reach an end volume of 200 μL. Then, 25-100 μg of nanobody-DTPA (1 mg/mL) was added and incubated for 30 min at RT. The radiolabeled nanobody solution was purified on a disposable Nap-5 gelfiltration column (GE Healthcare) and pushed through a 0.22 μm filter. Radiochemical purity was assessed using iTLC with 0.2 M citric acid as mobile phase, and with either analytical radio-HPLC or radio-SEC. Radio-HPLC was performed using a polystyrene divinylbenzene copolymer reversed-phase column (PLRP-S 300 Å, 5 μm, 250/4 mm, Agilent, Diegem, Belgium). Here, a mixture of 0.1% TFA in H₂O and ACN was used as eluent with the following gradient: 0-5 min 25% ACN; 5-7 min 25-34% ACN; 7-10 min 75-100% ACN; 10-25 min 100% ACN at a flow rate of 1 ml / min. Radio-SEC was done on Superdex 75 5/150GL using PBS as mobile phase at a flow rate of 0.3 mL / min.

Untagged ¹¹¹In-DTPA-2Rs15d, used for dynamic planar scintigraphy studies, consisted of a nanobody: ¹¹¹In ratio of 7:1. For the *ex vivo* biodistribution experiments with untagged ¹⁷⁷Lu-DTPA-2Rs15d a ratio of

9:1 (nanobody:¹⁷⁷Lu) was achieved, while for targeted radionuclide therapy, samples of untagged ¹⁷⁷Lu-DTPA-2Rs15d with a nanobody:¹⁷⁷Lu ratio of 3:1 were used.

Preparation of ¹⁷⁷Lu-DTPA-Trastuzumab

Conjugation of 1B4M-DTPA to Trastuzumab was performed based on the protocol described by Sampath and coworkers, to yield a DTPA:Trastuzumab ratio of 5:1 (34). Briefly, a 100-fold molar excess of bifunctional chelator 1B4M-DTPA was conjugated overnight at RT to the free ε-amino-groups of lysines in Trastuzumab (Herceptin®, Hoffman-La Roche, Missis-sauga, ON, USA) in 3500 μl of 0.05 M sodium carbonate buffer (pH 8.5). The reaction was quenched by reducing the pH to 7.0. DTPA-Trastuzumab was purified on Superdex 75 10/30 (GE Healthcare) in 0.1 M ammonium acetate buffer pH 7.0. The degree of conjugation was evaluated with ESI-Q-ToF-MS (Waters, Micromass), in positive mode. The necessary amount of ¹⁷⁷Lu was added to a test vial containing metal-free 0.1 M ammonium acetate buffer pH 5.0, to reach an end volume of 200 μL. Then, 100-250 μg DTPA-Trastuzumab (2.4 mg/mL) was added and incubated for 30 min at RT. ¹⁷⁷Lu-DTPA-Trastuzumab was purified on a disposable Nap-5 gelfiltration column (GE Healthcare) and pushed through a 0.22 μm filter. Radiochemical purity was assessed using iTLC and radio-SEC, as described above.

Animal Studies

Healthy male Wistar rats (255 ± 53 g body weight) were used in dynamic planar scintigraphy studies. Female athymic nude mice (20 ± 5 g body weight) were inoculated with 8 × 10⁶ SKOV3 cells in PBS, s.c. in the right hind leg, under 2.5 % isoflurane anesthesia (Abbott, Ottignies-Louvain-la-Neuve, Belgium). Tumors reached a size of 205 ± 68 mm³, for biodistribution purposes. SKOV3-LUC xenografts were obtained by inoculating female athymic mice with 3 × 10⁶ SKOV3-LUC cells in the right hind leg. Tumors were grown to reach 26 ± 5 mm³, for targeted radiotherapy purposes. The animal protocols were approved by the ethical committee of the Vrije Universiteit Brussel.

Kidney retention of ¹¹¹In-DTPA-nanobodies in healthy Wistar rats

Wistar rats (n=3) were anesthetized by an i.p. injection of 250 μL pentobarbital, prior to an i.v. injection of ¹¹¹In-DTPA-nanobodies (35.8 ± 5.4 MBq). In a separate group, the ¹¹¹In-DTPA-untagged nanobodies were additionally coinjected in parallel with 80 mg/kg Gelofusin (40 g/l, Braun Medical, Diegem,

Belgium). To record the fast *in vivo* kinetics of radio-labeled nanobodies, dynamic planar imaging was performed immediately after injection (100 frames of 30 s). Time activity curves of the kidneys were generated using AMIDE Medical Image Data Examiner software, as previously described (25). ROIs were drawn around total body and kidneys, to calculate the radioactivity retained in kidneys relative to the total injected activity (% IA).

In vivo tumor targeting of ¹⁷⁷Lu-DTPA-nanobodies

SKOV3 tumor-bearing mice (n=3) were injected i.v. with each of the ¹⁷⁷Lu-DTPA-2Rs15d nanobody formats (21.5 ± 1.7 MBq). In a separate group, ¹⁷⁷Lu-DTPA-untagged 2Rs15d was co-injected with 150 mg/kg Gelofusin. Mice were euthanized and dissected 1 h p.i., tissues were weighed and radioactivity was counted with an automated gamma counter (Cobra Inspector 5003, Canberra Packard, USA). The amount of radioactivity present in the different tissues was expressed as % IA/g tissue.

Comparative dosimetry calculation of a single dose ¹⁷⁷Lu-DTPA-untagged 2Rs15d and Gelofusin versus ¹⁷⁷Lu-DTPA-Trastuzumab

SKOV3 tumor-bearing mice were injected i.v. with either 14.7 ± 1.3 MBq ¹⁷⁷Lu-DTPA-untagged 2Rs15d and 150 mg/kg Gelofusin, or 10.1 ± 0.2 MBq ¹⁷⁷Lu-DTPA-Trastuzumab. At 1, 3, 6, 24, 48, 72, and 120 h p.i., mice (n=3) were euthanized and dissected to count radioactivity as described above and to obtain tissue biodistribution values expressed as % IA/g. The time point 168 h p.i. was included for the dosimetric calculation of ¹⁷⁷Lu-DTPA-Trastuzumab. These values were time integrated to obtain the residence time per gram tissue, following a procedure that was described elsewhere (26). Briefly, the integration between time 0 and 120 h (or 168 h for ¹⁷⁷Lu-DTPA-Trastuzumab) was made using the trapezoid method. The final 2 points were used to estimate the residence time from 120 h to infinity. For each data set, the absorbed doses were calculated. The S values of ¹⁷⁷Lu were obtained from RADAR phantoms (www.doseinfo-radar.com/RADARphan.html). The S value for 1 g sphere (0.0233 mGy/MBq s) was used for dose calculations.

Experimental targeted radionuclide therapy with ¹⁷⁷Lu-DTPA-untagged 2Rs15d and Gelofusin

When SKOV3-LUC tumors reached a volume of 20-30 mm³ (day 7), animals were randomly categorized into 3 groups (n=8). Mice in each group received 7 i.v. injections (once a week, over a period of 7 weeks)

of a volume containing either 20.7 ± 0.4 MBq ^{177}Lu -DTPA-untagged 2Rs15d, 19.3 ± 0.8 MBq ^{177}Lu -DTPA-untagged Bcl110, or PBS. All samples were diluted in 150 mg/kg Gelofusin. The study was terminated 125 days after tumor cell inoculation. Animal weights were monitored weekly, as well as tumor growth through caliper measurement. Once every 2 weeks, tumor burden was also visualized using bioluminescence imaging, after i.p. injection of 150 mg/kg Luciferin, according to Keyaerts and coworkers (21). Results were summarized in an event-free survival curve, with events defined as (1) mortality, (2) > 20 % weight loss, (3) ulcerating tumor tissue, or (4) a tumor volume exceeding 250 mm³. At the end of the study, animals were euthanized; dissected and renal tissues were preserved.

Kidney histopathology

Renal samples of ^{177}Lu -dosed and control groups were fixed in formalin for 4 hours, dehydrated and embedded in paraffin. The paraffin sections (3 μm) were processed for staining with H&E, PAS and Masson's trichrome, according to standard protocols. Stained sections were evaluated for necrosis, apoptosis, inflammation and vascular changes in the renal tissue, using light microscopy.

Statistics

Statistically significant differences in biodistribution were analyzed with the two-tailed t-test, while the event-free survival between treated groups was analyzed using the log-rank test ($P < 0.05$).

Results

Polarity of nanobodies

As nanobodies are predominantly cleared through the kidneys, these organs inevitably become the dose-limiting organs in targeted radionuclide therapy. Previous exploratory experiments indicated

that the C-terminal amino acid tag of the nanobody might have an important impact on the degree of kidney retention. Zimmerman polarity score plots of various 2Rs15d constructs are shown in figure 1. As compared to untagged 2Rs15d, the introduction of 6 histidines mark a high polar region at the C-terminus of His-tagged 2Rs15d. Myc-His-tagged 2Rs15d possesses an even higher C-terminal polarity score, due to the presence of an extra lysine, aspartic acid and 2 glutamic acids, all amino acids with a high polarity index value.

Conjugation of 1B4M-DTPA and CHX-A''-DTPA to nanobodies

CHX-A''-DTPA was used for ^{111}In labeling and 1B4M-DTPA for ^{177}Lu labeling. SEC profiles and ESI-Q-ToF-MS analyses indicated successful conjugation of the bifunctional DTPA-chelators to the different nanobody constructs. SEC profiles of untagged 2Rs15d, untagged 1B4M-DTPA-2Rs15d and untagged CHX-A''-DTPA-2Rs15d are presented in figure 2A-C. DTPA was conjugated to the ϵ -amino groups of lysine residues, hereby forming a thiourea bond. Therefore, since 2Rs15d contains multiple lysines, the conjugation reaction resulted in a mixture of molecules with 1, 2, and 3 DTPA chelators, as determined by ESI-Q-ToF-MS analysis. The MS profiles of untagged 2Rs15d (MW: 12624 Da), untagged CHX-A''-DTPA-2Rs15d (major peak corresponding to the conjugation of 2 DTPA, MW: 13923) and untagged 1B4M-DTPA-2Rs15d (major peak corresponding to the conjugation of 2 DTPA, MW: 13842) are shown in Additional file 1: supplementary figure 1. Consequently, the dominant conjugation ratio (chelator:nanobody) for both 1B4M-DTPA and CHX-A''-DTPA to untagged 2Rs15d is 2:1. By applying the standardized protocol, a consistent degree of 2:1 (chelator:nanobody) conjugation was also obtained for the nanobodies 2Rb17c and 1R136d.

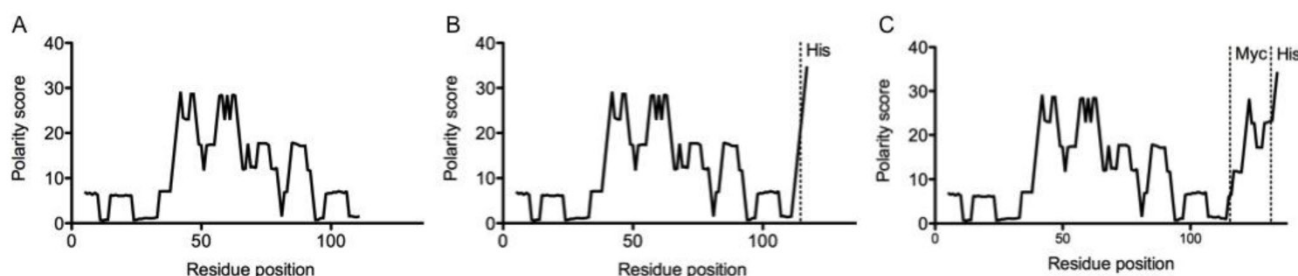


Figure 1: Zimmerman – polarity score plot for the various 2Rs15d nanobody formats. **(A)** untagged 2Rs15d; **(B)** His-tagged 2Rs15d and **(C)** Myc-His-tagged 2Rs15d. Introduction of charged amino acids at the nanobody's C-terminus has a major impact on the polarity score.

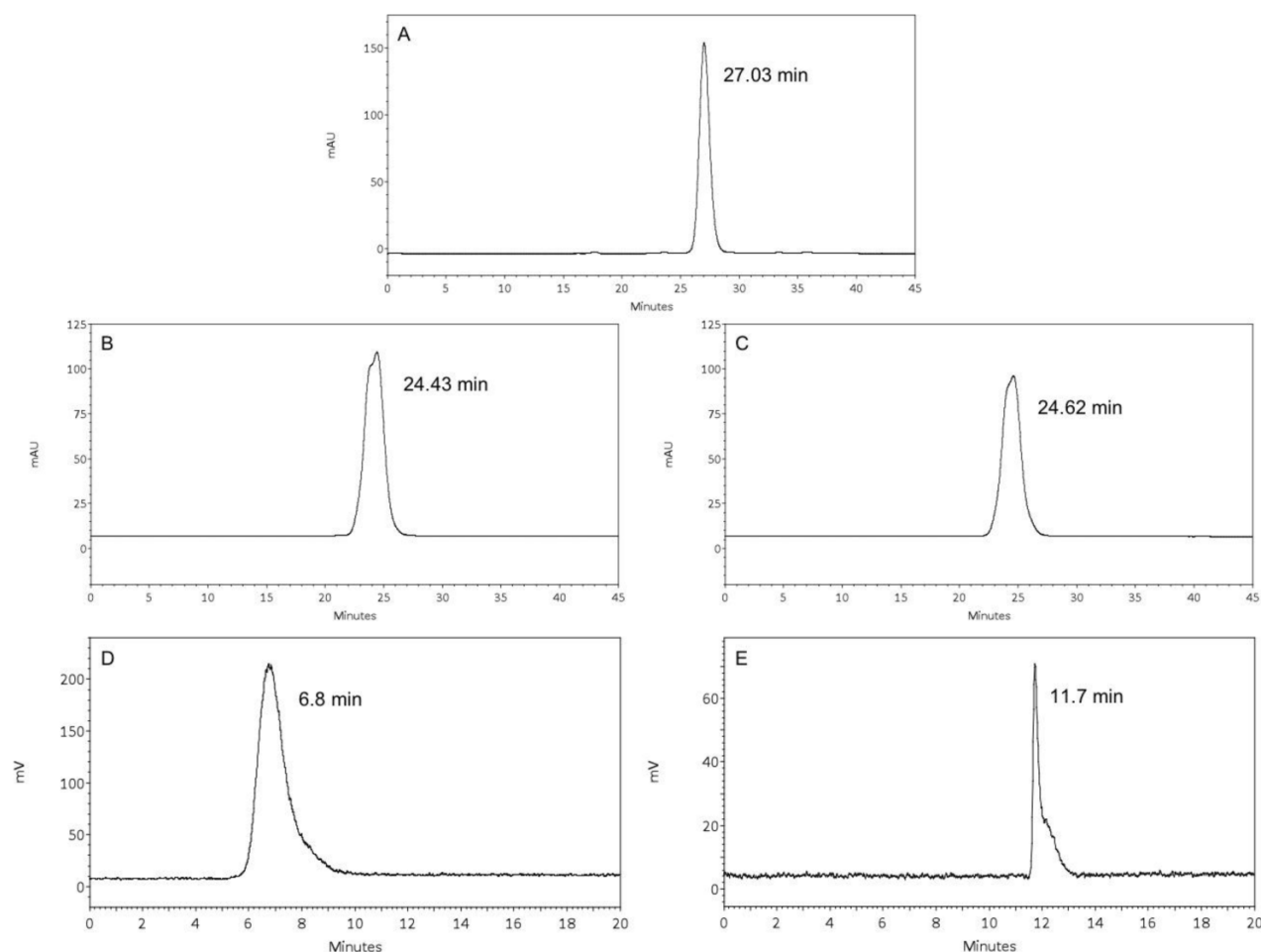


Figure 2: (Radio-)chromatographic analyses of various untagged 2Rs15d conjugates. **(A)** untagged nanobody, **(B)** CHX-A''-DTPA-2Rs15d, **(C)** 1B4M-DTPA-2Rs15d, **(D)** ^{177}Lu -DTPA-2Rs15d, **(E)** ^{111}In -DTPA-2Rs15d; **(A-C)** SEC on Superdex 10/30, **(D)** radio-SEC on Superdex 75 5/150GL; **(E)** radio-HPLC on PLRP-S. The R-times of the major peaks are shown in each graph.

Preparation of ^{111}In - and ^{177}Lu -DTPA-nanobodies

Nanobodies were conjugated with CHX-A''-DTPA for ^{111}In labeling. After radiolabeling, iTLC revealed radiochemical purities of $95.1 \pm 1.7\%$ and $> 99\%$, before and after SEC purification, respectively. The 2Rs15d nanobody constructs conjugated with 1B4M-DTPA were labeled with ^{177}Lu in high yields as determined by iTLC, i.e. $97.2 \pm 2.5\%$ before and $> 99\%$ after SEC purification. Radiochemical purities were confirmed with radio-HPLC or radio-SEC. The radio-HPLC profile of untagged ^{111}In -DTPA-2Rs15d and the radio-SEC profile of untagged ^{177}Lu -DTPA 2Rs15d are shown in figure 2D-E.

Preparation of ^{177}Lu -DTPA-Trastuzumab

SEC profiles and ESI-Q-ToF-MS analyses indicated successful conjugation of 1B4M-DTPA to Trastuzumab. The radiochemical purity of ^{177}Lu -DTPA-Trastuzumab was $99.5 \pm 0.2\%$ (iTLC) and was confirmed with radio-SEC. SEC profiles of untagged Trastuzumab and DTPA-Trastuzumab are

shown in Additional file 1: supplementary figure 2, together with the radio-SEC profile of ^{177}Lu -DTPA-Trastuzumab.

Kidney retention of ^{111}In -DTPA-nanobodies in healthy Wistar rats

To confirm that the nanobody's C-terminal polarity strongly influences the degree of kidney retention, Wistar rats were injected with the different ^{111}In -DTPA-nanobody constructs. Representative and equally scaled planar images are shown in figure 3A-D. Finally, whole-body and kidney ROIs were drawn and plotted as a function of time, to obtain the relative amounts of accumulating radioactivity in kidneys (Figure 3E). Highest accumulation of radioactivity in the kidneys was confirmed for Myc-His-tagged 2Rs15d, followed by His-tagged and untagged 2Rs15d, giving values of 52.44 ± 4.70 , 36.45 ± 4.28 and $18.24 \pm 1.71\%$ IA at 50 min p.i., respectively. All three curves described a similar parabolic shape. The lowest accumulation in kidneys was observed for untagged 2Rs15d that was coinfused with 80 mg/kg

Gelofusin, with a value of only 6.52 ± 0.18 % IA at 50 min p.i. Here the curve described an initial incline of radioactivity followed rapidly by a steady low amount of radioactivity in kidneys. These findings were confirmed for two additional HER2-targeting nanobodies 2Rb17c and 1R136d (Additional file 1: Supplementary Figure 3).

In vivo tumor targeting of the ^{177}Lu -DTPA-2Rs15d nanobodies

SKOV3 tumor xenografted mice (n=3) were injected with the different ^{177}Lu -DTPA-2Rs15d nanobodies. Tumor targeting was not affected by altering

the C-terminal tag or by a coinjection with gelofusin, with uptake values of 5.9 ± 0.7 %; 6.4 ± 0.8 %; 6.9 ± 0.4 % and 6.5 ± 0.2 % IA/g for Myc-His-tagged, His-tagged, untagged and untagged nanobody with 150 mg/kg Gelofusin, respectively. More importantly, again substantial differences in kidney uptake were observed, with decreasing values of 195.8 ± 23.7 %; 127.7 ± 2.9 %; 25.8 ± 1.3 % and 10.4 ± 1.7 % IA/g for Myc-His-tagged, His-tagged, untagged, and untagged nanobody together with 150 mg/kg Gelofusin, respectively (Figure 4). Uptake values in the major organs and tissues did not differ significantly.

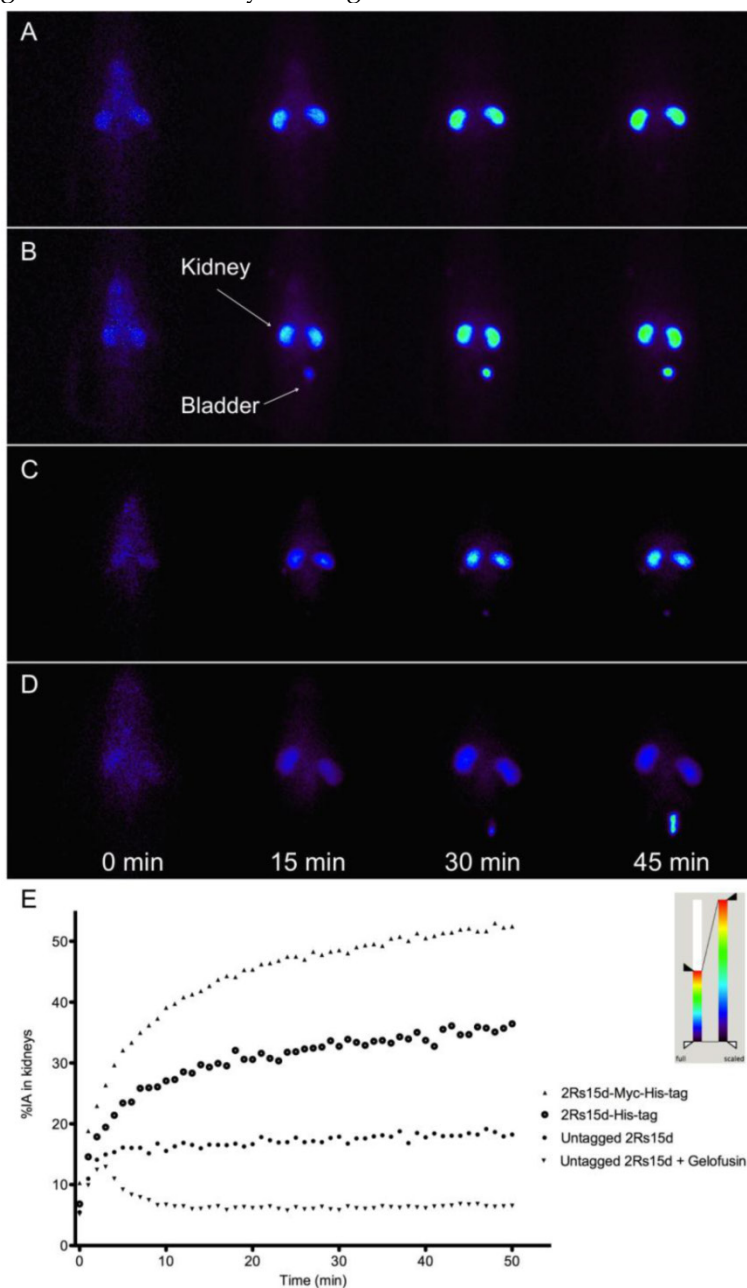


Figure 3: Accumulation of radioactivity in kidneys in function of time after injection of various ^{111}In -labeled 2Rs15d formats in healthy Wistar rats (n=3); (A-D) A selection of images are shown obtained by gamma camera dynamic scintigraphy; (A) 2Rs15d-Myc-His-tag, (B) 2Rs15d-His-tag, (C) untagged 2Rs15d, (D) untagged 2Rs15d confused with 80 mg/kg Gelofusin. (E) Time-activity curves of renal retention in rats (n=3 per condition). Lowest accumulation in kidneys was observed for the ^{111}In -labeled untagged 2Rs15d that was confused with 150 mg/kg Gelofusin.

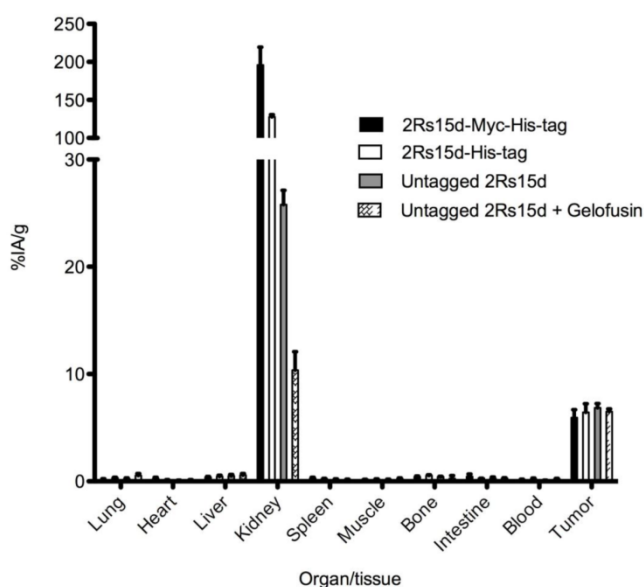


Figure 4: Ex vivo biodistribution analyses of ¹⁷⁷Lu-labeled 2Rs15d constructs in HER2^{pos} tumor xenografted mice, at 1 h p.i. Animals were injected with 21.5 MBq (4 μg) radioconjugates. Columns, mean (n=3); bars, SD. Kidney accumulation decreased significantly by removing the C-terminal amino acid tag, and by a coinfusion with Gelofusin. Tumor targeting was not affected.

Comparative dosimetry calculation of a single dose ¹⁷⁷Lu-DTPA-untagged 2Rs15d and Gelofusin versus ¹⁷⁷Lu-DTPA-Trastuzumab

The biodistribution data are presented in Table 1. For untagged ¹⁷⁷Lu-DTPA-2Rs15d nanobody, the highest tumor uptake values were observed at early

time points and decreased from 6.50 ± 0.24 % IA/g at 1 h p.i. to 2.15 ± 0.11 % IA/g at 48 h p.i. and to 1.15 ± 0.16 % IA/g at 120 h p.i. Kidney uptake values peaked at 10.36 ± 1.73 % IA/g 1 h p.i. and then decreased to 2.08 ± 0.29 % IA/g at 48 h p.i. and 0.40 ± 0.29 % IA/g at 120 h p.i. Bone activity was low, indicating there was no substantial release of ¹⁷⁷Lu. Radioactivity concentration in the other major organs and tissues was low, with values below 0.5 % IA/g at early time points, and decreasing over time. In contrast, tumor uptake of ¹⁷⁷Lu-DTPA-Trastuzumab was low at early time points and increased from 1.07 ± 0.31 % IA/g to 28.09 ± 0.58 % IA/g at 96 h and 17.13 ± 2.00 % IA/g at 168 h p.i. Blood values were high with 23.32 ± 4.36 % IA/g at 1h and still 10.69 ± 1.77 % IA/g at 168 h p.i. At all-time points the radioactive concentrations in additional organs (especially in liver, lung and spleen) remained much higher than for untagged ¹⁷⁷Lu-DTPA-2Rs15d.

The dosimetry calculations are presented in table 2. For untagged ¹⁷⁷Lu-labeled 2Rs15d, the highest radiation absorbed dose was delivered to tumor and kidneys, with an equivalent value of 0.9 Gy/MBq, while the radiation burden to other healthy tissues was very low. ¹⁷⁷Lu-DTPA-Trastuzumab on the other hand delivered a calculated dose to the tumor of 5.55 Gy/MBq. However, radiation to blood, liver, spleen and lung was also high and estimated to be 4.18, 1.72, 1.60 and 1.55 Gy/MBq, respectively.

Table 1. Ex vivo biodistribution of (A) untagged ¹⁷⁷Lu-DTPA-2Rs15d nanobody coinfused with 150 mg/kg Gelofusin and (B) ¹⁷⁷Lu-DTPA-Trastuzumab, in HER2^{pos} xenografted mice (n=3 per time point).

Organ	1 h p.i.		3 h p.i.		6 h p.i.		24 h p.i.		48 h p.i.		72 h p.i.		96 h p.i.		120 h p.i.		168 h p.i.	
	Mean ± SD	Mean ± SD	Mean ± SD	Mean ± SD	Mean ± SD	Mean ± SD	Mean ± SD	Mean ± SD	Mean ± SD	Mean ± SD	Mean ± SD	Mean ± SD	Mean ± SD	Mean ± SD	Mean ± SD	Mean ± SD	Mean ± SD	
A Lung	0.53 ± 0.19	0.13 ± 0.02	0.06 ± 0.02	0.04 ± 0.01	0.02 ± 0.02	0.03 ± 0.01	0.02 ± 0.004	0.03 ± 0.01	0.02 ± 0.004	0.03 ± 0.01	0.03 ± 0.01	0.03 ± 0.01	0.03 ± 0.01	0.03 ± 0.01	0.01 ± 0.01	0.02 ± 0.02	N/A ± N/A	N/A ± N/A
Heart	0.12 ± 0.04	0.05 ± 0.01	0.03 ± 0.03	0.04 ± 0.01	0.02 ± 0.03	0.03 ± 0.01	0.02 ± 0.003	0.02 ± 0.001	0.03 ± 0.001	0.02 ± 0.001	0.03 ± 0.001	0.03 ± 0.01	0.01 ± 0.01	0.01 ± 0.01	0.01 ± 0.01	0.01 ± 0.01	N/A ± N/A	N/A ± N/A
Liver	0.57 ± 0.15	0.50 ± 0.27	0.22 ± 0.08	0.28 ± 0.10	0.11 ± 0.01	0.09 ± 0.02	0.10 ± 0.03	0.05 ± 0.02	0.10 ± 0.03	0.05 ± 0.03	0.05 ± 0.03	0.05 ± 0.03	0.05 ± 0.03	0.05 ± 0.03	0.05 ± 0.03	0.05 ± 0.03	N/A ± N/A	N/A ± N/A
Kidney	10.36 ± 1.73	7.59 ± 0.71	6.86 ± 0.23	4.33 ± 1.13	2.08 ± 0.29	1.98 ± 0.12	1.32 ± 0.21	0.40 ± 0.29	2.08 ± 0.29	1.98 ± 0.12	1.32 ± 0.21	0.40 ± 0.29	0.40 ± 0.29	0.40 ± 0.29	0.40 ± 0.29	0.40 ± 0.29	N/A ± N/A	N/A ± N/A
Spleen	0.16 ± 0.05	0.07 ± 0.02	0.07 ± 0.004	0.07 ± 0.02	0.04 ± 0.01	0.04 ± 0.01	0.04 ± 0.01	0.04 ± 0.01	0.04 ± 0.01	0.04 ± 0.01	0.04 ± 0.01	0.04 ± 0.01	0.04 ± 0.01	0.04 ± 0.01	0.04 ± 0.01	0.04 ± 0.01	N/A ± N/A	N/A ± N/A
Muscle	0.22 ± 0.09	0.08 ± 0.03	0.06 ± 0.004	0.03 ± 0.01	0.02 ± 0.004	0.03 ± 0.01	0.02 ± 0.004	0.03 ± 0.01	0.02 ± 0.004	0.03 ± 0.01	0.02 ± 0.01	0.02 ± 0.01	0.02 ± 0.01	0.01 ± 0.01	0.01 ± 0.01	0.01 ± 0.01	N/A ± N/A	N/A ± N/A
Bone	0.26 ± 0.28	0.21 ± 0.06	0.17 ± 0.02	0.10 ± 0.04	0.06 ± 0.01	0.06 ± 0.01	0.05 ± 0.04	0.05 ± 0.01	0.06 ± 0.01	0.06 ± 0.01	0.05 ± 0.04	0.05 ± 0.01	0.05 ± 0.01	0.05 ± 0.01	0.05 ± 0.01	0.05 ± 0.01	N/A ± N/A	N/A ± N/A
Intestine	0.28 ± 0.05	0.13 ± 0.08	0.06 ± 0.03	0.04 ± 0.02	0.03 ± 0.01	0.02 ± 0.01	0.02 ± 0.01	0.02 ± 0.01	0.03 ± 0.01	0.02 ± 0.01	0.02 ± 0.01	0.02 ± 0.01	0.02 ± 0.002	0.01 ± 0.01	0.01 ± 0.01	0.01 ± 0.01	N/A ± N/A	N/A ± N/A
Blood	0.21 ± 0.06	0.01 ± 0.004	0.01 ± 0.002	0.003 ± 0.002	0.001 ± 0.001	0.001 ± 0.001	0.002 ± 0.001	0.001 ± 0.001	0.002 ± 0.001	0.002 ± 0.001	0.001 ± 0.001	0.001 ± 0.001	0.001 ± 0.001	0.001 ± 0.001	0.001 ± 0.001	0.001 ± 0.001	N/A ± N/A	N/A ± N/A
Tumor	6.50 ± 0.24	5.97 ± 0.43	4.29 ± 0.09	3.58 ± 0.32	2.15 ± 0.11	2.93 ± 0.58	2.07 ± 1.09	1.15 ± 0.16	2.15 ± 0.11	2.93 ± 0.58	2.07 ± 1.09	1.15 ± 0.16	1.15 ± 0.16	1.15 ± 0.16	1.15 ± 0.16	1.15 ± 0.16	N/A ± N/A	N/A ± N/A
B Lung	4.65 ± 0.92	6.60 ± 0.33	6.30 ± 0.93	4.34 ± 0.33	4.43 ± 1.05	4.83 ± 0.66	4.72 ± 1.30	3.76 ± 0.54	4.65 ± 0.92	6.60 ± 0.33	6.30 ± 0.93	4.34 ± 0.33	4.43 ± 1.05	4.83 ± 0.66	4.72 ± 1.30	3.76 ± 0.54	4.14 ± 1.22	4.14 ± 1.22
Heart	5.29 ± 1.25	4.85 ± 0.61	4.48 ± 0.31	3.15 ± 0.34	3.00 ± 0.69	2.66 ± 1.19	2.32 ± 0.32	2.53 ± 0.31	5.29 ± 1.25	4.85 ± 0.61	4.48 ± 0.31	3.15 ± 0.34	3.00 ± 0.69	2.66 ± 1.19	2.32 ± 0.32	2.53 ± 0.31	2.07 ± 0.30	2.07 ± 0.30
Liver	6.46 ± 0.48	5.37 ± 1.72	5.49 ± 0.91	4.99 ± 1.00	4.91 ± 0.48	5.59 ± 0.43	5.10 ± 1.47	5.53 ± 1.47	6.46 ± 0.48	5.37 ± 1.72	5.49 ± 0.91	4.99 ± 1.00	4.91 ± 0.48	5.59 ± 0.43	5.10 ± 1.47	5.53 ± 1.47	4.96 ± 0.60	4.96 ± 0.60
Kidney	5.77 ± 1.99	4.43 ± 0.85	3.45 ± 0.17	4.13 ± 0.27	3.51 ± 0.99	3.60 ± 1.10	3.77 ± 0.77	3.46 ± 0.26	5.77 ± 1.99	4.43 ± 0.85	3.45 ± 0.17	4.13 ± 0.27	3.51 ± 0.99	3.60 ± 1.10	3.77 ± 0.77	3.46 ± 0.26	2.57 ± 0.67	2.57 ± 0.67
Spleen	5.64 ± 0.99	4.12 ± 0.40	4.12 ± 0.06	4.50 ± 0.70	4.45 ± 0.95	4.78 ± 1.20	5.17 ± 1.45	6.46 ± 0.79	5.64 ± 0.99	4.12 ± 0.40	4.12 ± 0.06	4.50 ± 0.70	4.45 ± 0.95	4.78 ± 1.20	5.17 ± 1.45	6.46 ± 0.79	5.12 ± 1.51	5.12 ± 1.51
Muscle	0.71 ± 0.25	0.81 ± 0.28	1.16 ± 0.36	1.47 ± 0.20	1.57 ± 0.18	0.88 ± 0.28	1.25 ± 0.62	1.18 ± 0.10	0.71 ± 0.25	0.81 ± 0.28	1.16 ± 0.36	1.47 ± 0.20	1.57 ± 0.18	0.88 ± 0.28	1.25 ± 0.62	1.18 ± 0.10	2.51 ± 0.38	2.51 ± 0.38
Bone	1.56 ± 0.16	1.59 ± 0.24	2.29 ± 0.11	2.53 ± 0.42	2.43 ± 0.37	2.30 ± 0.72	2.24 ± 0.15	2.40 ± 0.16	1.56 ± 0.16	1.59 ± 0.24	2.29 ± 0.11	2.53 ± 0.42	2.43 ± 0.37	2.30 ± 0.72	2.24 ± 0.15	2.40 ± 0.16	2.08 ± 0.09	2.08 ± 0.09
Intestine	2.84 ± 0.63	2.51 ± 0.25	1.72 ± 0.27	1.52 ± 0.38	1.51 ± 0.21	0.96 ± 0.27	1.17 ± 0.29	1.10 ± 0.25	2.84 ± 0.63	2.51 ± 0.25	1.72 ± 0.27	1.52 ± 0.38	1.51 ± 0.21	0.96 ± 0.27	1.17 ± 0.29	1.10 ± 0.25	0.90 ± 0.29	0.90 ± 0.29
Blood	23.32 ± 4.36	22.25 ± 2.80	18.87 ± 1.56	14.00 ± 1.29	12.58 ± 1.96	10.74 ± 1.18	10.69 ± 1.77	8.72 ± 0.88	23.32 ± 4.36	22.25 ± 2.80	18.87 ± 1.56	14.00 ± 1.29	12.58 ± 1.96	10.74 ± 1.18	10.69 ± 1.77	10.16 ± 1.40	8.72 ± 0.88	8.72 ± 0.88
Tumor	1.07 ± 0.31	1.62 ± 0.53	2.61 ± 0.74	7.89 ± 1.28	14.60 ± 1.80	22.85 ± 4.24	28.09 ± 0.58	17.13 ± 2.00	1.07 ± 0.31	1.62 ± 0.53	2.61 ± 0.74	7.89 ± 1.28	14.60 ± 1.80	22.85 ± 4.24	28.09 ± 0.58	19.59 ± 1.15	17.13 ± 2.00	17.13 ± 2.00

NOTE: Each data point presents an average ± SD and is expressed as % IA/g.

Table 2. Dosimetry calculation of untagged ^{177}Lu -DTPA-2Rs15d nanobody coinjected with 150 mg/kg Gelofusin, and of ^{177}Lu -DTPA-Trastuzumab, in HER2^{pos} xenografted mice.

Tissues	Untagged 2Rs15d	Trastuzumab
Lung	0.01	1.55
Heart	0.01	0.98
Liver	0.05	1.72
Kidney	0.90	1.22
Spleen	0.02	1.60
Muscle	0.01	0.41
Bone	0.03	0.77
Intestine	0.01	0.44
Blood	0.001	4.18
Tumor	0.90	5.55

NOTE: Dosimetry data are expressed as Gy/MBq

Experimental targeted radionuclide therapy with ^{177}Lu -DTPA-untagged 2Rs15d and Gelofusin

Mice bearing small SKOV3-LUC tumors were i.v. injected with either untagged ^{177}Lu -DTPA-2Rs15d, untagged ^{177}Lu -DTPA-BcII10 (a non-targeting control nanobody) or the vehicle PBS, all coinjected with 150 mg/kg Gelofusin. For both the PBS-treated (n=8) and ^{177}Lu -DTPA-BcII10-treated animals (n=8), the tumor volume of all animals already exceeded the value of 250 mm³ between day 33 and 75 after inoculation, as measured with a caliper (Figure 5B). All animals from the control groups were euthanized at day 85 due to the development of large tumors (> 1 cm³), as shown in Figure 5B. No statistically significant difference was observed in event-free survival between both control groups. In contrast, up to day 125 no substantial increase in tumor size was observed among the mice that were treated with untagged anti-HER2 ^{177}Lu -DTPA-2Rs15d (n=8). Remarkably, 5 out of 8 mice were completely free of tumor burden, as confirmed by bioluminescence imaging (Figure 5A). The other 3 mice developed small, LUC^{pos}, but no palpable tumors. One animal in this group had to be euthanized due to a weight loss of more than 20 % (day 95). Overall, event-free survival was significantly longer for the treated group compared to the control groups that received PBS (P < 0.0001) or ^{177}Lu -DTPA-BcII10 (P < 0.0001), respectively (Figure

6A). Histopathological analyses of renal tissues showed no differences between the experimental groups. The glomeruli, the tubuli and the vasculature were morphologically normal and no necrosis was noted. The interstitium was not broadened or fibrotic, and was free of inflammatory cells. No protein casts could be observed (figure 6B).

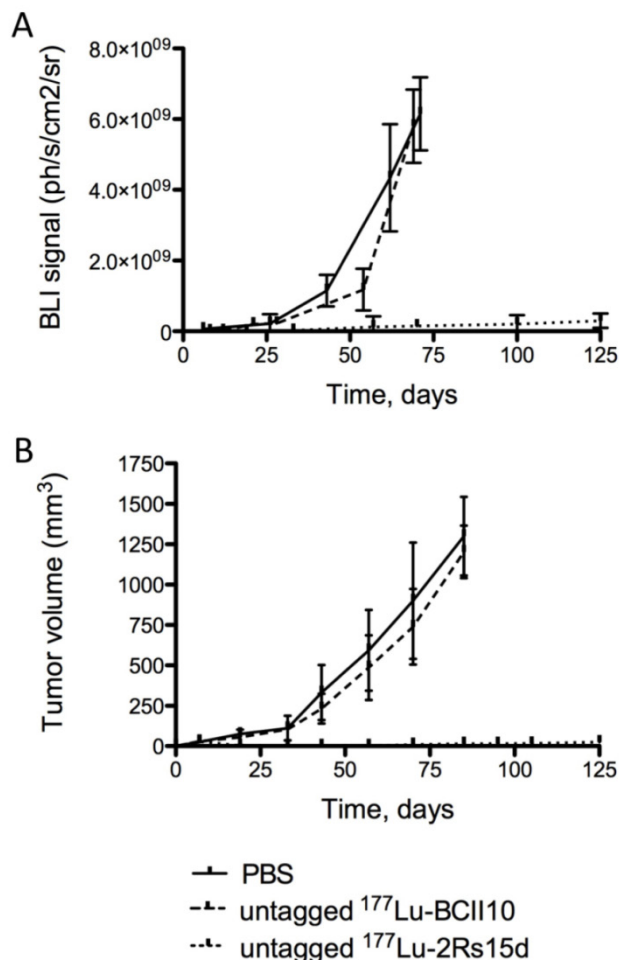


Figure 5: Tumor growth monitoring during targeted radionuclide therapy. Tumor volumes were quantified using (A) bioluminescence imaging (ph/s/cm²/sr) or (B) caliper measurements (mm³), in function of time (days). Animals (n=8 per group) were treated with a weekly injection of untagged ^{177}Lu -labeled 2Rs15d (20.7 ± 0.4 MBq) and in the control groups with PBS or ^{177}Lu -labeled BCII10 (19.3 ± 0.8 MBq). All treatments occurred with a 150 mg/kg Gelofusin coinjection. In terms of tumor growth, important differences were observed between both control groups and the treated group, for both caliper and bioluminescence measurements.

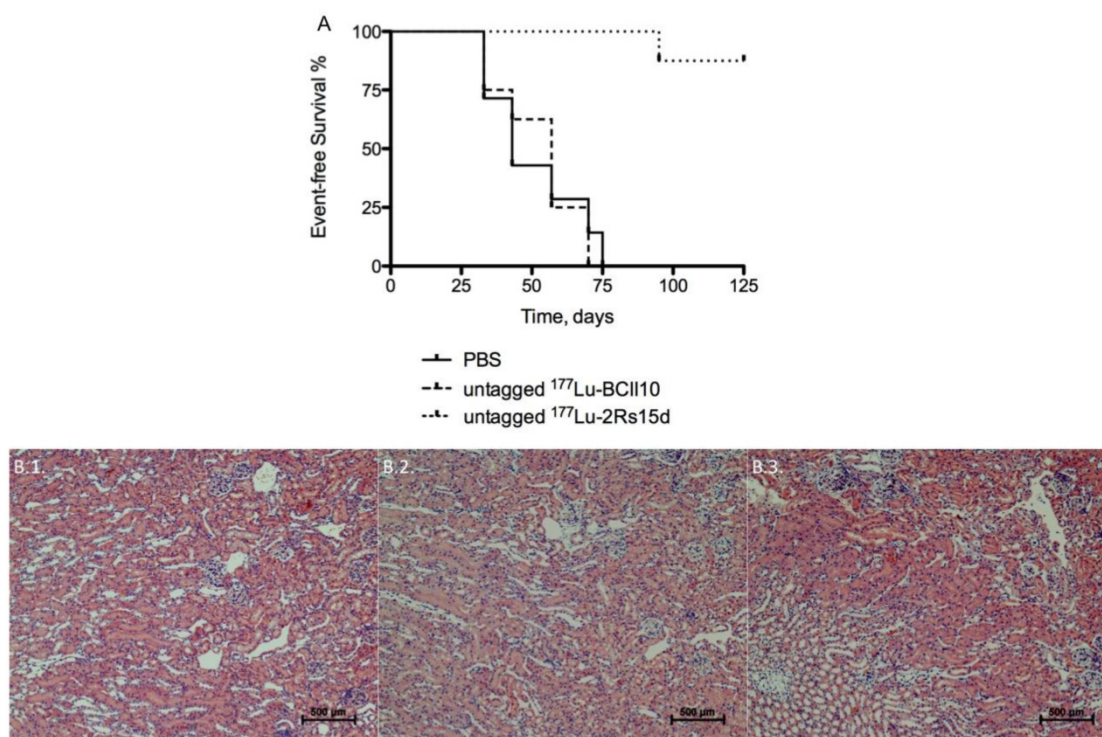


Figure 6: (A) Event-free survival during targeted radionuclide therapy. Events are defined as 1. Mortality; 2. > 20 % weight loss; 3. Ulcerating tumor tissue; 4. Tumor volume > 250 mm³. Animals (n=8 per group) were treated with a weekly injection of untagged ¹⁷⁷Lu-labeled 2Rs15d (20.7 ± 0.4 MBq) and in the control groups with PBS or ¹⁷⁷Lu-labeled BCII10 (19.3 ± 0.8 MBq). All treatments occurred with a 150 mg/kg Gelofusin coinjection. (B) Renal histopathology. Kidneys of ¹⁷⁷Lu-dosed animal groups were compared to the PBS-treated animal group. Sections were H&E stained and examined for evidence of renal toxicity. No differences in renal histology were observed between the animal groups that received (B.1) PBS, (B.2) untagged ¹⁷⁷Lu-labeled BCII10 or (B.3) untagged ¹⁷⁷Lu-labeled 2Rs15d.

Discussion

In the present study we describe nanobody-based targeted radionuclide therapy in tumor xenografted mice, using the therapeutic radionuclide ¹⁷⁷Lu. β-emitting radionuclides such as ¹⁷⁷Lu produce particles with a mean energy of 0.1-1 MeV and a range of 1-10 mm, and possess the ability to target multiple cell diameters. Effective antibody-based RIT applications are still limited, as mAbs show poor tumor penetration and non-specific accumulation of radioactivity in organs and tissues, with bone marrow toxicity as the major dose-limiting factor (myelotoxicity). In 2005, Persson and coworkers presented an experimental study on ¹⁷⁷Lu-labeled anti-HER2 mAb Pertuzumab in HER2^{pos} tumor xenografted mice (28). Here, high accumulation in tumor tissue was measured, with values of 8 % IA/g and 20 % IA/g at day 1 and 3 respectively. However, at these time points blood values were still at 8 % IA/g and 3 % IA/g. At day 1 values of 3-5 % IA/g were measured in organs like kidney, liver and spleen, which only slowly decreased over time. More recently, Ray and coworkers described similar observations in a biodistribution study with ¹⁷⁷Lu-labeled anti-HER2 mAb Trastuzumab versus a non-specific ¹⁷⁷Lu-labeled mAb HulgG in

HER2^{pos} xenografted mice (27). Although high tumor uptake values were observed using ¹⁷⁷Lu-Trastuzumab (16.24 ± 4.18 % IA/g at 24 h p.i. and 19.08 ± 3.23 % IA/g at 48 h p.i.), they also registered tumor uptake values of 7.51 ± 1.98 and 7.41 ± 0.73 % IA/g at the same time points after injecting ¹⁷⁷Lu-HulgG. Moreover, non-specific accumulation in healthy tissues remained high at all-time points, with still 10.06 ± 2.75 % IA/g in blood and 6.70 ± 1.71, 5.69 ± 2.12, and 4.24 ± 0.62 % IA/g in respectively liver, spleen and kidney, 96 h after injecting ¹⁷⁷Lu-Trastuzumab. We confirmed these data by performing an *ex vivo* biodistribution analyses of ¹⁷⁷Lu-DTPA-Trastuzumab in SKOV3 xenografted mice. Tumor uptake of ¹⁷⁷Lu-DTPA-Trastuzumab was low at early time points and increased from 1.07 ± 0.31 % IA/g to 28.09 ± 0.58 % IA/g at 96 h and 17.13 ± 2.00 % IA/g at 168 h p.i. Blood values were high with 23.32 ± 4.36 % IA/g at 1h and still 8.72 ± 0.88 % IA/g at 168 h p.i. Highly perfused organs like liver, lung, kidney and spleen showed significant retention of radioactivity up to 168 h p.i.

Different alternatives aiming to compensate for these limitations are currently under investigation: co-administration of anti-angiogenic agents, extracorporeal elimination, pre-targeting, or engineering of

smaller antibody-derived vectors (1). The approach of smaller antibody-derived vectors is supported by their much faster target tissue accumulation and their low background retention of radioactivity. However, one drawback of using small molecular vectors remains the high kidney accumulation caused by intracellular entrapment of radioactivity due to non-specific tubular reuptake after glomerular filtration. We recently described successful radiolabeling of the His-tagged anti-HER2 nanobody 2Rs15d with ^{177}Lu , using the bifunctional chelator 1B4M-DTPA. Specific tumor targeting was observed, with low background tissue and organ uptake except for the kidneys, which was the main limitation for a clinical application of nanobody-based targeted radionuclide therapy (20). Therefore, finding countermeasures to reduce the degree of kidney retention was a main priority. Strategies to reduce the kidney uptake of radiolabeled protein- or peptide-based vectors have already been investigated intensively. For example, coinjection with a mixture of 150 mg/kg Gelofusin and 1.2 g/kg L-lysine could reduce renal uptake of a $^{99\text{m}}\text{Tc}$ -labeled anti-EGFR nanobody with 45 % (10). Gelofusin also reduced the kidney retention of radiolabeled octreotide analogs to a similar extent (29,30) and a combination of Gelofusin and L-lysine reduced kidney uptake even further (9,31). Alternatively, Wällberg and coworkers demonstrated that amino acid substitutions in the C-terminal amino acid sequence of an affibody molecule has a significant impact on the extent of kidney retention (8).

In this study we investigated the influence of the C-terminal amino acid tag on the overall polarity of the nanobody sequence on the one hand, and the degree of kidney retention on the other. Amino-acid tags are regularly linked to proteins such as antibody-fragments, for purification and radiolabeling purposes (His-tag) or for *in vitro* detection (Myc-tag). However, the introduction of potentially charged amino acids will affect the overall polarity of the protein, and thus also its *in vivo* behavior. This presumption was eventually confirmed by evaluating the *in vivo* behavior of different ^{111}In -DTPA-nanobody formats in healthy Wistar rats. The highest activity retained in kidneys was observed for Myc-His-tagged 2Rs15d. Changing Myc-His-tag to His-tag led to a drop in retention of label by 31 %, 50 min p.i. complete removal of the C-terminal amino acid tag lowered kidney retention up to 65 %, as compared to the Myc-His-tagged 2Rs15d. Finally, coinjecting untagged ^{111}In -DTPA-2Rs15d with Gelofusin further reduced kidney retention with an additional 65 %. This observation was confirmed with two other HER2-targeting nanobodies.

A similar trend was observed after injecting the different 2Rs15d formats, radiolabeled with ^{177}Lu , in HER2^{pos} xenografted mice. Figure 4 confirms the observations from the dynamic scans regarding the kidney retention. The highest uptake value in kidney was observed for the Myc-His-tagged format whereas the lowest uptake was attained with the untagged 2Rs15d and 150 mg/kg Gelofusin. Tumor targeting was not affected by either adjusting the C-terminal amino acid tag or coinjecting Gelofusin.

A comparative *ex vivo* biodistribution of a single dose untagged ^{177}Lu -DTPA-2Rs15d with 150 mg/kg Gelofusin versus a single dose ^{177}Lu -DTPA-Trastuzumab was evaluated until 120 h and 168 h p.i., respectively. Injecting untagged ^{177}Lu -DTPA-2Rs15d nanobody revealed a fast washout of activity from all non-target organs and tissues. At 48 h p.i., the radioactivity in tumor exceeded the amount present in kidney, resulting in a comparable radiation absorbed dose to tumor and kidneys. The dose delivered to non-targeted tissues like blood, liver, and spleen were extremely low. Moreover, the low dose delivered to bone suggests the absence of free ^{177}Lu . In contrast, although ^{177}Lu -DTPA-Trastuzumab supplied a 6 fold higher dose to the tumor than untagged ^{177}Lu -DTPA-2Rs15d, also the radiation burden to lung, liver, spleen, bone and blood was concomitantly 155, 34, 80, 26 and 4180 fold higher.

In 2004, Adams and coworkers reported RIT in HER2^{pos} xenografts using an Yttrium-90 labeled anti-HER2 diabody (32). Despite the use of a different radioisotope in this study (Indium-111 for imaging, Yttrium-90 for RIT), they observed important differences in *ex vivo* biodistribution compared to our results with untagged ^{177}Lu -DTPA 2Rs15d nanobody. Although tumor uptake values, measured for the diabody, were higher in the SKOV3 xenograft model (double at 24 h p.i.), non-specific accumulation was also much higher in kidney (7 fold), blood (500 fold), spleen (33 fold) and liver (13 fold), all at 24 h p.i., resulting in observed toxicity in kidneys.

Finally, nanobody-based targeted radionuclide therapy was performed in HER2^{pos} xenografted mice with small tumor volumes of 20-30 mm³, as a preliminary model to mimic minimal residual or micrometastatic disease. Both experimental groups receiving either non-specific ^{177}Lu -labeled BcII10 nanobody or the vehicle PBS group noted no significant differences in terms of tumor growth inhibition. Tumor volumes of all animals in both control groups exceeded already the value of 250 mm³ between day 33 and 75 after inoculation. No animals in the treated group had tumors exceeding 250 mm³ up to day 125. Moreover, 5 out of the 8 treated mice showed complete absence of tumor formation. The other 3 mice developed small,

but no palpable tumors, that were however detectable via bioluminescence imaging.

Taken together, the results presented here show a successful application of nanobody-based targeted radionuclide therapy in tumor-bearing mice, using the therapeutic radionuclide Lutetium-177. Since highly specific nanobodies are easily raised against a variety of cancer-related antigens, nanobody-based targeted radionuclide therapy could be introduced in several types of cancer disease.

Conclusion

We have demonstrated that kidney retention is reduced significantly when using untagged nanobodies and coinfusion with 150 mg/kg Gelofusin. Hence, anti-HER2 nanobodies constitute potent small molecular vehicles for targeted radionuclide therapy. Anti-HER2 nanobodies, when radiolabeled with ¹⁷⁷Lu, efficiently inhibit growth of HER2 expressing tumors in xenografted mice, without pronounced non-specific radiation to healthy tissues. Moreover, histopathological analyses of renal tissue revealed no visible toxicity.

Supplementary Material

Additional File 1:

Supplementary Figures 1-3.

<http://www.thno.org/v04p0708s1.pdf>

Abbreviations

RIT: radioimmunotherapy; mAbs: monoclonal antibodies; Molecular Weight: MW; C-terminal: carboxyl-terminal; PRRT: peptide receptor radionuclide therapy; CEA: carcino-embryonic antigen; EGFR: epidermal growth factor receptor; HER2: human epidermal growth factor receptor 2; PSMA: prostate-specific membrane antigen; His-tag: hexahistidine-tag; ¹⁷⁷Lu: Lutetium-177; Immuno-PET: immuno-positron emission tomography; PBS: phosphate-buffered saline; ¹¹¹In: Indium-111; ESI-Q-ToF-MS: Electrospray ionization quadrupole time-of-flight mass spectrometry; RT: room temperature; iTLC: instant Thin Layer Chromatography; R-time: retention time; HPLC: High Performance Liquid Chromatography; SEC: size-exclusion chromatography; TFA: Trifluoroacetic acid; ACN: acetonitrile; Da: Dalton; s.c.: subcutaneous; i.p.: intraperitoneal; i.v.: intravenous; ROIs: regions of interest; p.i.: post-injection; ^{99m}Tc: Technetium-99m; H&E: hematoxylin and eosin; PAS: Periodic acid-Schiff; SPECT: Single Photon Emission Computed Tomography; SD: standard deviation; %IA/g: % injected activity per gram tissue; N/A: not available; Gy/MBq: Gray per Megabecquerel.

Acknowledgments

The 1B4M-DTPA bifunctional chelator was generously donated by Dr. Martin Brechbiel (National Cancer Institute, Bethesda, TX, USA). Matthias D'Huyvetter is funded by a SCK•CEN/VUB grant and the foundation Emmanuel van der Schueren. Tony Lahoutte is a Senior Clinical Investigator of the Research Foundation – Flanders (Belgium) (FWO). The research at ICMI is funded by the Belgian State, Nationaal Kankerplan, Vlaamse Liga tegen Kanker and Vlaamse Stichting tegen Kanker. This work was also supported by FWO-Vlaanderen (Research Project G.013910). We thank Karine Breckpot for providing the luciferase^{pos} cell line, and Cindy Peleman and Arnaud Campsteyn for technical assistance.

Competing Interests

The authors have declared that no competing interest exists.

References

- Jain M, Gupta S, Kaur S, Ponnusamy MP, Batra SK. Emerging Trends for Radioimmunotherapy in Solid Tumors. *Cancer Biother Radiopharm.* 2013; [Epub ahead of print]
- Huhlov A, Chester KA. Engineered single chain antibody fragments for radioimmunotherapy. *Q J Nucl Mol Imaging.* 2004;48:279-88.
- Christensen EL, Brin H. Megalin and cubulin: multifunctional endocytic receptors. *Nat Rev Mol Cell Biol.* 2002;3:256-266.
- De Jong M, Barone R, Krenning E, Bernard B, Melis M, Visser T, Gekle M, Willnow TE, Walrand S, Jamar F, Pauwels S. Megalin is essential for renal proximal tubule reabsorption of (111)In-DTPA-octreotide. *J Nucl Med.* 2005;46:1696-1700.
- Moll S, Nিকেleit V, Mueller-Brand J, Brunner FP, Maecke HR, Mihatsch MJ. A new cause of renal thrombotic microangiopathy: yttrium 90-DOTATOC internal radiotherapy. *Am J Kidney Dis.* 2001;37:847-51.
- Stoffel MP, Pollok M, Fries J, Baldamus CA. Radiation nephropathy after radiotherapy in metastatic medullary thyroid carcinoma. *Nephrol Dial Transplant.* 2001;16:1082-3.
- Barone R, Borson-Chazot F, Valkema R, Walrand S, Chauvin F, Gogou L, et al. Patient-specific dosimetry in predicting renal toxicity with 90Y-DOTATOC: relevance of kidney volume and dose rate in finding a dose-effect relationship. *J Nucl Med.* 2005;46:99S-106S.
- Wällberg H, Orlova A, Altai M, Hosseinimehr SJ, Widström C, Malmberg J, Ståhl S, Tolmachev V. Molecular design and optimization of 99mTc-labeled recombinant affibody molecules improves their biodistribution and imaging properties. *J Nucl Med.* 2011;52(3):461-9.
- Rolleman EJ, Bernard BF, Breenman WA, Forrer F, de Blois E, Hoppin J, et al. Molecular imaging of reduced renal uptake of radiolabelled [DOTA0,Tyr3]octreotate by the combination of lysine and gelofusine in rats. *Nuklearmedizin.* 2008;47:110-5.
- Gainkam LO, Caveliers V, Devoogdt N, Vanhove C, Xavier C, Boerman O, Muyltermans S, Bossuyt A, Lahoutte T. Localization, mechanism and reduction of renal retention of technetium-99m labeled epidermal growth factor receptor-specific nanobody in mice. *Contrast Media Mol Imaging.* 2011;6(2):85-92.
- Hamers-Casterman C, Atarhouch T, Muyltermans S, et al. Naturally occurring antibodies devoid of light chains. *Nature.* 1993;363:446-448.
- Vaneycken I, D'huyvetter M, Hernot S, De Vos J, Xavier C, Devoogdt N, Caveliers V, Lahoutte T. Immuno-imaging using nanobodies. *Curr Opin Biotechnol.* 2011 Dec;22(6):877-81.
- Vaneycken I, Govaert J, Vincke C, Caveliers V, Lahoutte T, De Baetselier P, Raes G, Bossuyt A, Muyltermans S, Devoogdt N. In vitro analysis and in vivo tumor targeting of a humanized, grafted nanobody in mice using pinhole SPECT/micro-CT. *J Nucl Med.* 2010 Jul;51(7):1099-106.
- Gainkam LO, Huang L, Caveliers V, Keyaerts M, Hernot S, Vaneycken I, Vanhove C, Revets H, De Baetselier P, Lahoutte T. Comparison of the biodistribution and tumor targeting of two 99mTc-labeled anti-EGFR nanobodies in mice, using pinhole SPECT/micro-CT. *J Nucl Med.* 2008 May;49(5):788-95.
- Vaneycken I, Devoogdt N, Van Gassen N, Vincke C, Xavier C, Wernery U, Muyltermans S, Lahoutte T, Caveliers V. Preclinical screening of anti-HER2 nanobodies for molecular imaging of breast cancer. *FASEB J.* 2011 Jul;25(7):2433-46.

16. Xavier C, Vaneycken I, D'Huyvetter M, Heemskerk J, Keyaerts M, Vincke C, Devoogdt N, Muyltermans S, Lahoutte T, Caveliers V. Synthesis, Preclinical Validation, Dosimetry, and Toxicity of ⁶⁸Ga-NOTA-Anti-HER2 Nanobodies for iPET Imaging of HER2 Receptor Expression in Cancer. *J Nucl Med*. 2013; [Epub ahead of print]
17. Evazalipour M, D'Huyvetter M, Soltani Tehrani B, Abolhassani M, Omidfar K, Abdoli S, Arezumand R, Morovvati H, Lahoutte T, Muyltermans S, Devoogdt N. Generation and characterization of nanobodies targeting PSMA for molecular imaging of prostate cancer. *Contrast Media and Molecular Imaging* 2013; Accepted.
18. Hynes NE, Lane HA. ERBB receptors and cancer: the complexity of targeted inhibitors. *Nat Rev Cancer*. 2005;5:341-35.
19. Yarden Y. Biology of HER2 and its importance in breast cancer. *Oncology*. 2001;61(2):1-13.
20. D'Huyvetter M, Aerts A, Xavier C, Vaneycken I, Devoogdt N, Gijs M, Impens N, Baatout S, Ponsard B, Muyltermans S, Caveliers V, Lahoutte T. Development of ¹⁷⁷Lu-nanobodies for radioimmunotherapy of HER2-positive breast cancer: evaluation of different bifunctional chelators. *Contrast Media Mol Imaging*. 2012;7(2):254-64.
21. Keyaerts M, Verschuere J, Bos TJ, Tchouate-Gainkam LO, Peleman C, Breckpot K, Vanhove C, Caveliers V, Bossuyt A, Lahoutte T. Dynamic bioluminescence imaging for quantitative tumour burden assessment using IV or IP administration of D-¹²⁵I-luciferin: effect on intensity, time kinetics and repeatability of photon emission. *Eur J Nucl Med Mol Imaging*. 2008;35(5):999-1007.
22. Broisat A, Hernot S, Toczek J, De Vos J, Riou LM, Martin S, Ahmadi M, Thielens N, Wernery U, Caveliers V, Muyltermans S, Lahoutte T, Fagret D, Ghezzi C, Devoogdt N. Nanobodies Targeting Mouse/Human VCAM1 for the Nuclear Imaging of Atherosclerotic Lesions. *Circulation Res*. 2012;110:927-937.
23. Saeuens D, Pellis M, Loris R, Pardon E, Dumoulin M, Matagne A, Wyns L, Muyltermans S, Conrath K. Identification of a universal VHH framework to graft non-canonical antigen-binding loops of camel single-domain antibodies. *J Mol Biol*. 2005;352(3):597-607.
24. Zimmerman JM, Eliezer N, Simha R. The characterization of amino acid sequences in proteins by statistical methods. *J Theor Biol*. 1968;21(2):170-201.
25. Hmila I, Cosyns B, Tounsi H, Roosens B, Caveliers V, Abderrazek RB, Bou-baker S, Muyltermans S, El Ayeb M, Bouhaouala-Zahar B, Lahoutte T. Pre-clinical studies of toxin-specific Nanobodies: Evidence of in vivo efficacy to prevent fatal disturbances provoked by scorpion envenoming. *Toxicol Appl Pharmacol*. 2012;264(2):222-31.
26. Tolmachev V, Orlova A, Pehrson R, Galli J, Baastrup B, Andersson K, Sandström M, Rosik D, Carlsson J, Lundqvist H, Wennborg A, Nilsson FY. Radio-nuclide therapy of HER2-positive microxenografts using a ¹⁷⁷Lu-labeled HER2-specific antibody molecule. *Cancer Res*. 2007;67(6):2773-2782.
27. Ray GL, Baidoo KE, Keller LMM, Albert PS, Brechbiel MW, Milenic D. Pre-clinical assessment of ¹⁷⁷Lu-labeled trastuzumab targeting HER2 for treatment and management of cancer patients with disseminated intraperitoneal disease. *Pharmaceuticals*. 2012;5:1-15.
28. Persson M, Tolmachev V, Andersson K, Gedda L, Sandström M, Carlsson J. [¹⁷⁷Lu]pertuzumab: experimental studies on targeting of HER-2 positive tumour cells. *Eur J Nucl Med Mol Imaging*. 2005;32(12):1457-62.
29. van Eerd JE, Vegt E, Wetzels JF, Russel FG, Masereeuw R, Corstens FH, et al. Gelatin-based plasma expander effectively reduces renal uptake of ¹¹¹In-octreotide in mice and rats. *J Nucl Med*. 2006;47:528-33.
30. Vegt E, Wetzels JF, Russel FG, Masereeuw R, Boerman OC, van Eerd JE, et al. Renal uptake of radiolabeled octreotide in human subjects is efficiently inhibited by succinylated gelatin. *J Nucl Med*. 2006;47:432-36.
31. Gotthardt M, van Eerd-Vismale J, Oyen WJ, de Jong M, Zhang H, Rolleman E, et al. Indication for different mechanisms of kidney uptake of radiolabeled peptides. *J Nucl Med*. 2007;48:596-601.
32. Adams GP, Shaller CC, Dadachova E, Simmons HH, Horak EM, Tesfaye A, Klein-Szanto AJ, Marks JD, Brechbiel MW, Weiner LM. A single treatment of Yttrium-90-labeled CHX-A''-C6.5 diabody inhibits the growth of established human tumor xenografts in immunodeficient mice. *Cancer Res*. 2004;64:6200-6206.
33. Rasanah S, Rajabi H, Akhlaghpour S, Sheybani S. Radioimmunotherapy of mice bearing breast tumors with ¹⁷⁷Lu-labeled trastuzumab. *Turk J Med Sci*. 2012;42(1):1292-1298.
34. Sampath L, Kwon S, Ke S, Wang W, Schiff R, Mawad ME, Sevick-Muraca EM. Dual-labeled Trastuzumab-based imaging agent for the detection of human epidermal growth factor receptor 2 overexpression in breast cancer. *J Nucl Med*. 2007;48:1501-1510.